Journal of Molecular Liquids 371 (2023) 121068

Contents lists available at ScienceDirect

Journal of Molecular Liquids

journal homepage: www.elsevier.com/locate/molliq

Diffusivities of ketones and aldehydes in liquid ethanol by molecular dynamics simulations

Bruno Zêzere, Inês Portugal, Carlos M. Silva *, José R.B. Gomes *

CICECO – Aveiro Institute of Materials, Department of Chemistry, University of Aveiro, Campus Universitário, de Santiago, 3810-193 Aveiro, Portugal

ARTICLE INFO

Article history:
Received 22 September 2022
Revised 24 November 2022
Accepted 12 December 2022
Available online 15 December 2022

Keywords:
Aldehydes
Diffusion coefficient
Ethanol
Force field
Ketones
Molecular dynamics

ABSTRACT

The tracer diffusion coefficients of six ketones (propanone, butanone, pentan-2-one, pentan-3-one, hexan-2-one, hexan-3-one) and six aldehydes (methanal, ethanal, propanal, butanal, pentanal and hexanal) in liquid ethanol were computed by classical molecular dynamics (MD) simulations over 303.15–333.15 K and 1–150 bar. The calculated tracer diffusion coefficients, D_{12}^{MD}, compared very satisfactorily with experimental data from the literature, with average absolute relative deviations (AARD) between 9.48 % and 12.18 % for ketones, and between 6.30 % and 9.11 % for aldehydes. The trends of D_{12}^{MD} with solute size and temperature were accurately simulated in all cases, while the weaker influence of pressure was not rigorously reached in all cases when jumping from 1 to 75 bar and then to 150 bar. Furthermore, a temperature-based correction to D_{12}^{MD} was introduced, which decreased the AARD values of ketones to the range 1.52–5.16 % and aldehydes to 2.94–3.45 %. The analyses of the spatial distribution functions and coordination numbers show that ethanol has more affinity with ketones than with aldehydes, though such affinity difference is not always translated to the computed D_{12}^{MD} of ketone-aldehyde isomers. Nevertheless, the experimental diffusivities of both families of compounds are only *ca.* 7 % different, hence within the uncertainties associated with the calculated results.

1. Introduction

Diffusion results from the spontaneous random thermal movement of species in a mixture and can be quantified in terms of diffusion coefficients (D). These properties are of chief importance not only for fundamental research but also for design and optimization of rate-controlled industrial processes [1,2].

Over the past years several phenomenological models and computational approaches have been developed for estimation and correlation of self-diffusion (D_{11}) and tracer binary diffusion coefficients (D_{12}). The D_{11} and D_{12} properties correspond to the diffusivity where, in the case of the former, the solute and the solvent are species of the same kind (label 1), while in the latter an infinitely diluted solute (label 2) moves through a distinct solvent (label 1).

In terms of phenomenological modeling, one may refer i) the analytical equations such as those of Liu-Silva-Macedo [3–6] for prediction and correlation of D_{11} and D_{12}; ii) the Dymond-Hildebrand-Batschinski (DHB) correlation [7,8] for D_{11} and D_{12} data correlation; iii) the Wilke-Chang equation [9] for D_{12} prediction; iv) and the Rice and Gray approaches for D_{12} correlation [10,11]. Recently, machine learning (ML) approaches based on different physicochemical descriptors have also been employed, such as i) the works by Aniceto *et al.* for D_{12} estimation in supercritical CO_2 [12] or in polar and nonpolar fluids [13] or ii) by Allers *et al.* for prediction of D_{11} in Lennard Jones fluids [14]. Moreover, artificial neural networks for D_{11} prediction in model and real fluids [15] have also been employed.

In terms of computational approaches, molecular dynamics (MD) simulations, either based on classical mechanics [16–19] or quantum mechanics [20], were employed to derive trajectories, from which diffusivities are calculated from the slope of the mean square displacement (MSD) over a time interval according to the Einstein relation [21]:

$$D^{MD} = \lim_{t\to\infty} \frac{[r(t_0+t) - r(t_0)]^2}{6t} \quad (1)$$

where D^{MD} is the diffusion coefficient computed from the MD simulations, t_0 is the time origin, and t is the elapsed time from t_0. While the correlations and artificial intelligence methods are very useful and computationally cheap, their effective applicability is limited by the quality and diversity of the data available, in terms of the number and nature of the systems and set of conditions used in their experimental measurement. Therefore, with the objective of

* Corresponding authors.
E-mail addresses: carlos.manuel@ua.pt (C.M. Silva), jrgomes@ua.pt (J.R.B. Gomes).

https://doi.org/10.1016/j.molliq.2022.121068
0167-7322/

obtaining diffusivity data for more complex molecular systems, the computational chemistry approaches become interesting alternatives. Nonetheless, the MD simulations also have some associated problems, such as the lack of appropriate potential parameters (a.k.a. force fields) for those based in classical mechanics, or the significant computational effort required for those based on quantum mechanics, even if the molecular systems consider a few dozens of molecules.

In the past few decades, relevant efforts have been performed to parametrize force fields with parameters that are highly transferable, like OPLS [22], GROMOS [23] or GAFF [24]. Consequently, the quality of simulations targeting systems that were not considered during the parametrization becomes quite satisfactory, with the OPLS force field being considered to model successfully different organic solutes. For instance, Skarmoutsos *et al.* [25] studied the solvation and diffusion of caffeine in supercritical (SC) mixtures of CO_2 and ethanol using the OPLS and EPM2 force fields; Vaz *et al.* [19] computed D_{12}^{MD} of various ketones in SC-CO_2 using the OPLS and EPM2 force fields achieving good agreement with experimental data; Lee *et al.* [26] studied the diffusivity of benzene and water in SC-CO_2 using the OPLS, TIP4P/2005 and EPM2 force fields, respectively, with satisfactory results achieved; and Khanal and Adhikari [27] computed D_{12}^{MD} of amoxicillin in ethanol using the OPLS force field. Despite the simplicity of non-polarizable force fields, they have been used to study quite complex systems, such as in the work by Guevara-Carrion *et al.* [28] where it was studied the diffusion of multicomponent mixtures of water/methanol/ethanol/propan-2-ol using rigid, non-polarizable, force fields based on Lennard–Jones sites.

Tracer binary diffusion coefficients can be experimentally measured using different methods, namely, solid dissolution (SD) technique [29], photon correlation spectroscopy (PCS) [29], radioactive tracer response (RTR) [29], nuclear magnetic resonance (NMR) [30], and, most commonly, by chromatographic methods among which we have the chromatographic peak broadening (CPB) (also called Taylor-Aris) technique [31–35], the modified Taylor-Aris technique, and the chromatographic impulse response (CIR) method [36–38]. However, the experimental measurement of D_{12} is expensive, time consuming and requires specific equipment that very often operates under limited range of conditions. These difficulties lead to the lack of experimental data particularly regarding D_{12} in dense systems, with less than 10,000 data points available in the literature, of which less than 3000 are of systems with polar solvents [11]. Hence, computational approaches become increasingly relevant to estimate diffusivities of non-studied or partially studied systems. In the last case, the D_{12}^{MD} values are computed for operating conditions not yet covered in previous studies, and the quality of the calculated values can be ascertained upon comparison with available experimental data.

This study is devoted to the simulation of D_{12}^{MD} of six ketones and six aldehydes in compressed liquid ethanol. The ketones considered are propanone, butanone, pentan-2-one, pentan-3-one, hexan-2-one, hexan-3-one, while the aldehydes are methanal, ethanal, propanal, butanal, pentanal and hexanal. The main goal of the work is the evaluation of a computational strategy using classical MD simulations for D_{12}^{MD} determination of the selected ketones and aldehydes in liquid ethanol, at temperatures from 303.15 K to 333.15 K and pressures up to 150 bar. This is accomplished upon comparison of the calculated values (D_{12}^{MD}) with experimental data (D_{12}^{exp}) available for the same conditions. Additionally, the influence of temperature and pressure on the computed diffusivities is investigated alongside the differences or similarities found between isomers. The solute–solvent interactions are also analyzed by inspecting structural properties of the systems like spatial distribution functions and coordination numbers. These simulations are expected to contribute to the understanding of transport phenomenon of compounds with carbonyl functional group.

2. Computational methods

The MD simulations carried out in this work were performed with the GROMACS 2019 [39–41] code considering the OPLS-AA (optimized potentials for liquid simulations – all atoms) [22] force field for all compounds. This force field was selected due to its versatility, existence of a vast number of parameters in the literature, compatibility and easiness of implementation, and also because it was previously found to enable the calculation of diffusivities of other compounds, such as, D_{12}^{MD} of amoxicillin in water and ethanol [27], D_{11}^{MD} of different solvents like *n*-decane, *n*-hexadecane, *n*-octacosane, ethanol, 1-decanol, cyclohexane, benzene, 2-methylpentane, 2,2-dimethylbutane, ethyl butanoate, and *n*-hexanoic acid [42], and D_{12}^{MD} of C3-C5 ketones in SC-CO_2 [19], which were in good agreement with available experimental results. Preliminary calculations for some selected systems also supported our choices as shown below.

In the OPLS-AA force field, the potential energy of the non-bonded interactions ($V_{non-bonded}$) are calculated based on the Lennard-Jones and Coulomb potentials by:

$$V_{non-bonded} = 4\varepsilon_{ij}\left[\left(\frac{\sigma_{ij}}{r_{ij}}\right)^{12} - \left(\frac{\sigma_{ij}}{r_{ij}}\right)^{6}\right] + \frac{q_i q_j}{4\varepsilon_r r_{ij}} \quad (2)$$

where r_{ij} is the distance between atoms *i* and *j*, ε_{ij} is the well depth potential energy between *i* and *j* at $r_{ij} = 2^{\frac{1}{6}}\sigma_{ij}$, σ_{ij} is the distance between *i* and *j* at which the potential is null, q_i ($1\,e = 1.602176565 \times 10^{-19}$C) is the charge of atom *i* or *j*, and ε_r is the relative permittivity. The σ_{ij} and ε_{ij} are calculated from their single values using geometric combining rules:

$$\sigma_{ij} = \left(\sigma_i \sigma_j\right)^{1/2} \quad (3)$$

$$\varepsilon_{ij} = \left(\varepsilon_i \varepsilon_j\right)^{1/2} \quad (4)$$

The potential energy of the bonded interactions is calculated from the stretching vibration of bonds ($V_{stretching}$), bending vibration of bonds (V_{angle}), and internal torsions ($V_{dihedrals}$):

$$V_{stretching} = k_{ij}/2\left(r_{ij} - r_0\right)^2 \quad (5)$$

where r_0 is the equilibrium bond length, and k_{ij} is the force constant of stretching vibrations;

$$V_{angle} = k_{ikj}/2\left(\theta_{ikj} - \theta_0\right)^2 \quad (6)$$

where θ_0 is the equilibrium angle between three atoms, k_{ikj} is the force constant of bending vibrations and θ_{ikj} is the angle between the atoms;

$$V_{dihedrals} = \sum_{n=0}^{5} k_n\left(\cos\left(\theta_{ijkl} - 180\right)\right)^n \quad (7)$$

where k_n are the function coefficients, and θ_{ijkl} is the torsion angle. The OPLS-AA bonding and non-bonded parameters used in this work can be found in Tables SD1–SD4 (Supplementary Data).

The MD simulations used cubic boxes with 3500 molecules of ethanol and 10–29 molecules of the solute (Table SD5), resulting in mass concentrations between 0.5 % and 1 %. The simulations were carried out for each condition using the procedure suggested by Barrera and Jorge [18]: first, the simulation was initialized by a

steepest descent minimization run; this was followed by a 100 ps run in the canonical ensemble (NVT), with initial velocities generated according to the Maxwell distribution; then, a 100 ps run in the isothermal–isobaric ensemble (NPT) was carried out using the Berendsen coupling scheme [43]; finally, the simulation continued in the NPT ensemble up to a few nanoseconds (see below). The final stage was carried out using the leap-frog algorithm [44], and the box temperature and pressure were kept constant by using the V-rescale temperature-coupling thermostat [45] and the Parrinello-Rahman barostat [46], respectively. Additionally, the LINCS algorithm was used to constrain the bond lengths and a cut-off distance of 1.4 nm was adopted for both van der Walls and Coulomb interactions. This cut-off value was selected previously by Vaz *et al.* [19] for obtaining tracer diffusivities of ketones in SC-CO_2, and confirmed in this work to enable the calculation of diffusivities that compared well with those obtained with larger cut-off values of 1.6 nm and 1.8 nm (Table SD6), and also with the available experimental data (Table SD6). The particle-mesh Ewald (PME) [47] summation was selected for the long-range electrostatic interactions. The compressibility values were taken from Ref. [48], and when not available their values were estimated by the correlation of Ref. [49]. The total time of the simulations was 6 ns, with a time step of 0.001 ps. Unless when noticed, the first 3 ns of equilibration were discarded and the other 3 ns were used for production as suggested by Vaz *et al.* [19]. The density values of the mixture were computed from the production phase and compared with the experimental data of pure ethanol whenever available. As it can be seen in Table SD7 for propanone in ethanol, the deviations were less than 1 %, which had to be expected for such low mass concentrations of the solute. Next, the diffusivities were computed performing a linear regression between 50 and 100 ps of the mean square displacements (MSD) as function of time, using all molecules in the simulation and all-time origins – the fitting procedure is illustrated in Fig. 1 for hexan-3-one in ethanol. Finally, the D_{12}^{MD} value was obtained dividing by six the slope of the fitted line as exemplified in Fig. 1b. For each combination of temperature and pressure, the computed properties are always the average of the results obtained from three independent simulations, *i.e.* three simulations with different starting conformations after randomly placing in the box the solute and solvent molecules.

Ideally, the selected region of the MSD used for fitting should have a slope of ~ 1 in the logarithmic MSD *versus* logarithmic t representation, which typically defines the diffusional region of the MSD [50]. From now on, the slope of the logarithmic MSD *versus* logarithmic t representation is defined as m_{log}. In this study, our decision of using always the same region enables the automatization of the process of calculation of the diffusivities for several systems and was triggered by previous work by Jamali *et al.* [51] that considered the 50–100 ps region for self-diffusivity calculations. We inspected in detail some of the systems and found that, despite the m_{log} values in the 50–100 ps region were slightly lower than the ideal value of 1 (with values going as low as 0.8), the fitting was performed away from the ballistic region of the MSD (typically presented in the initial region) occurring close to $t = 0$ as exemplified in Fig. 1b. Encouragingly, the diffusivities obtained from the fittings in the 50–100 ps region were found to compare very well with the results obtained from the first 50 ps time region showing $m_{log} \approx 1$ in the logarithmic MSD *versus* logarithmic t representation (Table SD8). As can be seen, for three simulation replicas of ethanolic solutions of hexan-2-one and butanal, at several different temperature and pressure conditions, the diffusivities obtained from the fittings in the 50–100 ps region or from the first 50 ps time region with m_{log} between 0.98 and 1.02, are the same within the uncertainties associated to the simulations. Importantly, the timing of the first region with $m_{log} \approx 1$ changes even in the case of simulation replicas for a given combination of temperature and pressure conditions. Therefore, based on the above findings and in order to make the procedure for the determination of the D_{12}^{MD} values as simple as possible, we decided to use the 50–100 ps fitting region for obtaining all the data discussed below.

We checked also the effect of the simulation time in the calculated diffusivities. We found that the results from 6 ns of simulation time were essentially the same as those calculated from much longer simulation runs, *i.e.* 40 ns of simulation (20 ns of equilibration followed by 20 ns of production), as can be seen in Table SD9 for acetone and butanone at 303.15 K, 318.15 K and 333.15 K and 1 bar, and butanone at 303.15 K and 150 bar. Moreover, we compared also the effect of the ensemble. Within associated uncertainties, the diffusivities of propanone in ethanol at 303.15 K and 1 bar from NVT and NPT simulations were the same, the values being, respectively $D_{12}^{MD} = 2.03 \times 10^{-5} \pm 0.11 \times 10^{-5}$ cm^2 s^{-1} and $D_{12}^{MD} = 1.97 \times 10^{-5} \pm 0.06 \times 10^{-5}$ cm^2 s^{-1}. Because we wanted to compare calculated data with experimental results at

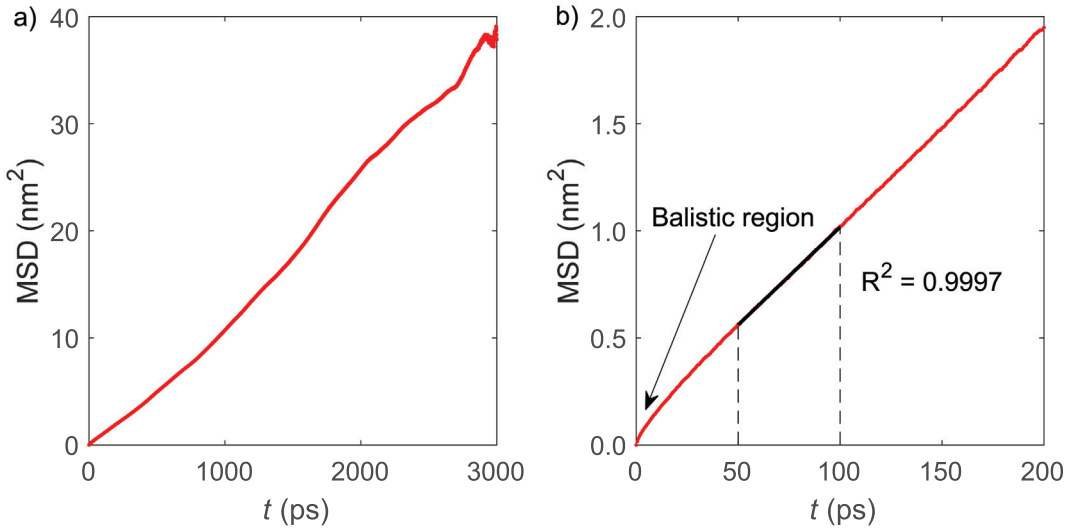

Fig. 1. Mean square displacement (MSD) of hexan-3-one in ethanol at 303.15 K and 1 bar during the production phase (3 ns): (a) full MSD function against time; (b) representation of the fitted section, between 50 and 100 ps. Symbols: – fitting line; • calculated MSD.

controlled temperature and pressure conditions, the NPT ensemble was used to obtain the data discussed below.

The quality of the data that arose from the simulations was assessed in terms of the relative deviation (RD), average relative deviation (ARD), and average absolute relative deviation (AARD) against the available experimental data through the expressions below:

$$RD(\%) = \frac{D_{12}^{MD} - D_{12}^{exp}}{D_{12}^{exp}} \quad (8)$$

$$ARD(\%) = \frac{100}{NDP}\sum_{i=1}^{NDP}\left(\frac{D_{12}^{MD} - D_{12}^{exp}}{D_{12}^{exp}}\right)_i \quad (9)$$

$$AARD(\%) = \frac{100}{NDP}\sum_{i=1}^{NDP}\left|\frac{D_{12}^{MD} - D_{12}^{exp}}{D_{12}^{exp}}\right|_i \quad (10)$$

3. Results and discussion

The computed D_{12}^{MD} can be found in Tables 1 and 2 alongside the relative deviation to the experimental data [52]. Overall, the results found for the aldehydes and ketones in liquid ethanol are satisfactory. In the case of the ketones, the global AARD values are between 9.48 % and 12.18 %, while for the aldehydes they are between 6.30 % and 9.11 %. The maximum deviation (25.32 %) is found for butanone at 333.15 K and 150 bar. In the following, the MD simulations are discussed and compared with the experimental data.

3.1. Comparison of calculated and experimental diffusivities

For both ketones and aldehydes, it is clear that RD increases with temperature though there is a major difference between the two families of compounds. In the former, the RD values at 303.15 K are mostly positive, ranging from as low as −3.88 % to 8.33 %, with an ARD of 1.98 % (systematic deviations are also evident in Fig. 2). In contrast, the RD of aldehydes are mostly negative at this temperature, ranging from −8.77 % to 0.72 %, with ARD value of −4.50 % (systematic deviations are also evident in Fig. 3). As for the highest temperature, 333.15 K, the deviations found for the ketones lie between 6.64 % and 25.32 %, with ARD = 19.22 %, while for aldehydes the deviations are lower, ranging from 10.71 % to 16.94 % with ARD = 13.70 %. This error increment with temperature may be attributed to the fact that the parameterization and validation of the OPLS-AA force field were done against experimental properties obtained at conditions close to 298.15 K [22]. Hence, bigger deviations may be expected as one departs from this temperature. In fact, such deviations were also observed in other classical MD studies using OPLS-based force fields. For example, Klein *et al.* found that the difference between the L-OPLS-AA calculated and experimental density of liquid *n*-dodecane increased with the temperature increase in the interval 298.15–573.15 K [53]. In a very recent study with the OPLS4 force field by Baba *et al.* [54], it was found that the self-diffusion coefficients of 152 liquids were clearly affected by the temperature variation. These observations emphasize that a single set of parameters that work well for a given temperature may not work well for other different conditions. In fact, in the case of the studied ketones, an increment of 30 K is enough to deviate the calculated D_{12}^{MD} over 20 % from the experimental value, which is further evidenced in Fig. 2. Even though RD increases with T, the effect over D_{12}^{MD} is always correctly translated. As temperature increases, the energy and the free volume of the system increase, therefore the diffusion coefficient also increases. This observation is valid at all pressures and for all studied solutes.

Concerning the influence of pressure, the diffusivities from the MD simulations do not evidence a clear trend as the values in Tables 1-2 demonstrate. Theoretically, as pressure increases, the solvent molecules become more packed and the free volume for diffusion decreases, which subsequently penalizes D_{12}. For instance, from 1 to 150 bar, the D_{12}^{MD} values always decrease, even though the translated differences are not as expressive as they should (*i.e.,* pentan-2-one at 333.15 K). However, the pressure effect is not always followed as shown for butanone at 333.15 K, since D_{12}^{MD} decreases from 1 to 75 bar and increases from 75 to 150 bar. One may conclude the weak influence of pressure on diffusivity is within the uncertainty associated to the data calculated

Table 1
Computed diffusion coefficients (D_{12}^{MD}) of ketones in liquid ethanol at various temperatures (T) and pressures (P). Values in parenthesis are deviations to the experimental data [52].

		Propanone	Butanone	Pentan-2-one	Pentan-3-one	Hexan-2-one	Hexan-3-one
T (K)	P (bar)	$D_{12}^{MD} \pm \Delta D_{12}^{MD}$ (10^{-5} cm^2 s^{-1})					
303.15	1	1.97 ± 0.06 (1.55 %)	1.75 ± 0.05 (0.00 %)	1.60 ± 0.13 (1.91 %)	1.62 ± 0.01 (2.53 %)	1.49 ± 0.11 (2.76 %)	1.56 ± 0.06 (8.33 %)
303.15	75	1.89 ± 0.04 (2.72 %)	1.67 ± 0.04 (1.21 %)	1.51 ± 0.14 (2.72 %)	1.51 ± 0.05 (– %)	1.32 ± 0.06 (-2.22 %)	1.39 ± 0.05 (– %)
303.15	150	1.81 ± 0.15 (2.26 %)	1.61 ± 0.05 (2.55 %)	1.48 ± 0.04 (6.47 %)	1.34 ± 0.03 (– %)	1.24 ± 0.05 (-3.88 %)	1.29 ± 0.08 (0.78 %)
318.15	1	2.72 ± 0.06 (14.29 %)	2.31 ± 0.11 (6.94 %)	2.13 ± 0.05 (9.79 %)	2.11 ± 0.05 (– %)	1.84 ± 0.05 (3.37 %)	1.98 ± 0.20 (– %)
318.15	75	2.43 ± 0.06 (8.97 %)	2.24 ± 0.02 (9.27 %)	2.08 ± 0.10 (13.66 %)	2.11 ± 0.05 (– %)	1.89 ± 0.06 (12.50 %)	1.94 ± 0.01 (– %)
318.15	150	2.36 ± 0.20 (11.32 %)	2.07 ± 0.03 (6.70 %)	1.95 ± 0.13 (12.72 %)	1.99 ± 0.07 (– %)	1.75 ± 0.02 (10.76 %)	1.78 ± 0.06 (– %)
333.15	1	3.57 ± 0.10 (23.53 %)	3.16 ± 0.14 (20.15 %)	2.57 ± 0.17 (6.64 %)	2.80 ± 0.23 (15.23 %)	2.50 ± 0.19 (14.68 %)	2.61 ± 0.08 (20.28 %)
333.15	75	3.34 ± 0.32 (22.79 %)	2.84 ± 0.15 (13.15 %)	2.78 ± 0.04 (25.23 %)	2.53 ± 0.20 (– %)	2.40 ± 0.16 (18.23 %)	2.33 ± 0.05 (– %)
333.15	150	3.14 ± 0.14 (22.18 %)	2.97 ± 0.09 (25.32 %)	2.55 ± 0.06 (21.43 %)	2.42 ± 0.14 (– %)	2.30 ± 0.16 (19.17 %)	2.37 ± 0.10 (20.30 %)
	ARD	12.18 %	9.48 %	11.17 %	(– %)	8.37 %	(– %)
	AARD	12.18 %	9.48 %	11.17 %	(– %)	9.73 %	(– %)

Table 2
Computed diffusion coefficients (D_{12}^{MD}) of aldehydes in liquid ethanol at various temperatures (T) and pressures (P). Values in parenthesis are deviations to the experimental data [52].

		Methanal	Ethanal	Propanal	Butanal	Pentanal	Hexanal
T (K)	P (bar)	$D_{12}^{MD} \pm \Delta D_{12}^{MD}$ (10^{-5} cm^2 s^{-1})					
303.15	1	3.07 ± 0.05	2.49 ± 0.05	2.08 ± 0.10	1.84 ± 0.08	1.63 ± 0.08	1.50 ± 0.04
		(– %)	(– %)	(– %)	(-5.15 %)	(-4.68 %)	(-2.60 %)
303.15	150	2.65 ± 0.08	2.28 ± 0.14	1.89 ± 0.09	1.56 ± 0.10	1.44 ± 0.10	1.40 ± 0.16
		(– %)	(– %)	(– %)	(-8.77 %)	(-6.49 %)	(0.72 %)
318.15	1	3.85 ± 0.13	3.28 ± 0.13	2.78 ± 0.16	2.40 ± 0.10	2.14 ± 0.08	1.99 ± 0.08
		(– %)	(– %)	(– %)	(2.13 %)	(0.00 %)	(6.42 %)
318.15	150	3.66 ± 0.11	2.93 ± 0.10	2.37 ± 0.11	2.16 ± 0.06	1.81 ± 0.04	1.75 ± 0.13
		(– %)	(– %)	(– %)	(4.85 %)	(-4.74 %)	(2.94 %)
333.15	1	5.09 ± 0.20	4.14 ± 0.17	3.56 ± 0.22	3.13 ± 0.29	2.78 ± 0.08	2.58 ± 0.12
		(– %)	(– %)	(– %)	(16.79 %)	(11.20 %)	(13.66 %)
333.15	150	4.62 ± 0.22	3.70 ± 0.20	3.11 ± 0.07	2.83 ± 0.15	2.48 ± 0.03	2.28 ± 0.02
		(– %)	(– %)	(– %)	(16.94 %)	(10.71 %)	(12.87 %)
	ARD	(– %)	(– %)	(– %)	4.46 %	1.00 %	5.67 %
	AARD	(– %)	(– %)	(– %)	9.11 %	6.30 %	6.53 %

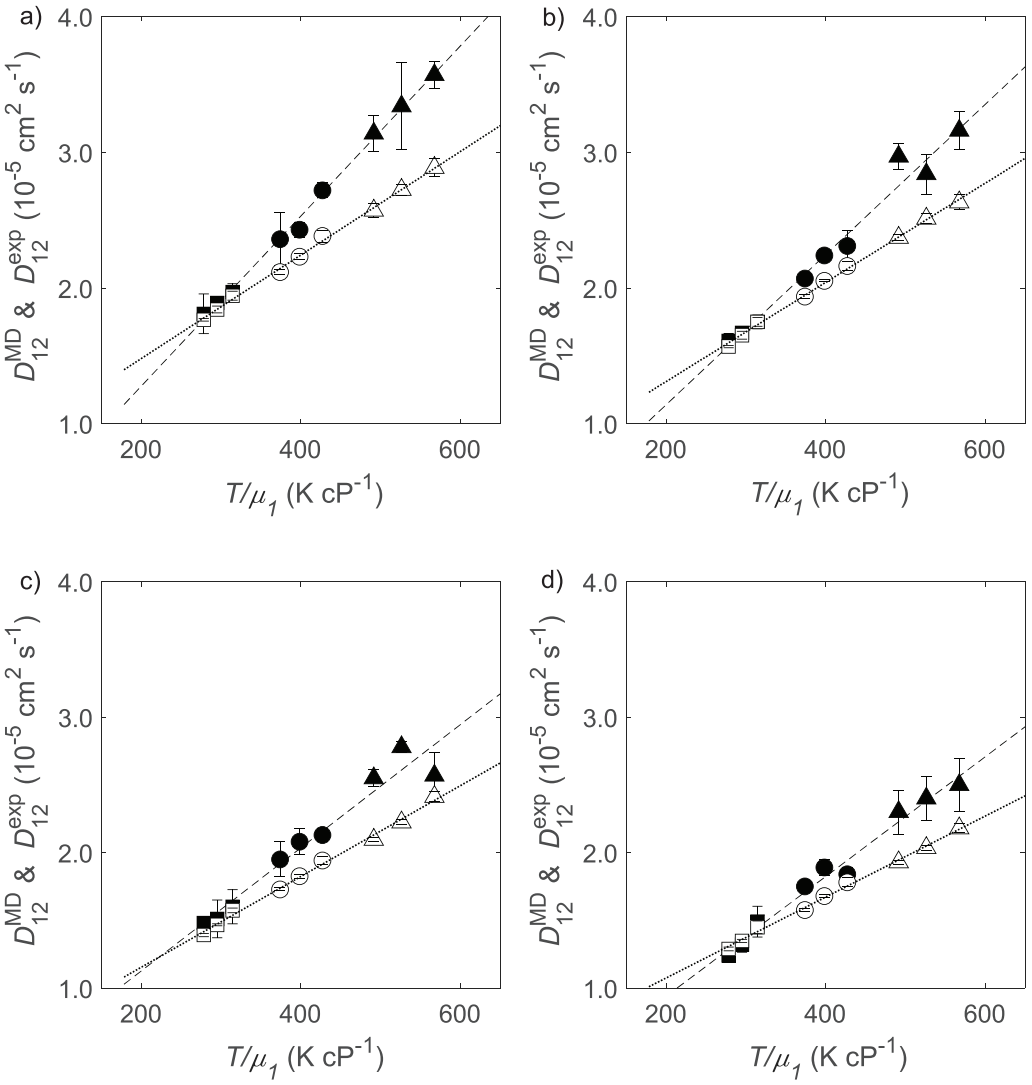

Fig. 2. Diffusion coefficients of ketones in liquid ethanol against hydrodynamic coordinates: filled symbols are D_{12}^{MD} values; open symbols are D_{12}^{exp} values from Ref. [52]. Values reported at 303.15 K (■ and □), 318.15 K (○ and ●) and 333.15 K (▲ and △) for (a) propanone, (b) butanone, (c) pentan-2-one and (d) hexan-2-one. The pentan-3-one and hexan-3-one results are omitted for simplicity. Viscosity values estimated by Mamedov equation as proposed by Cano-Gómez *et al.* [55].

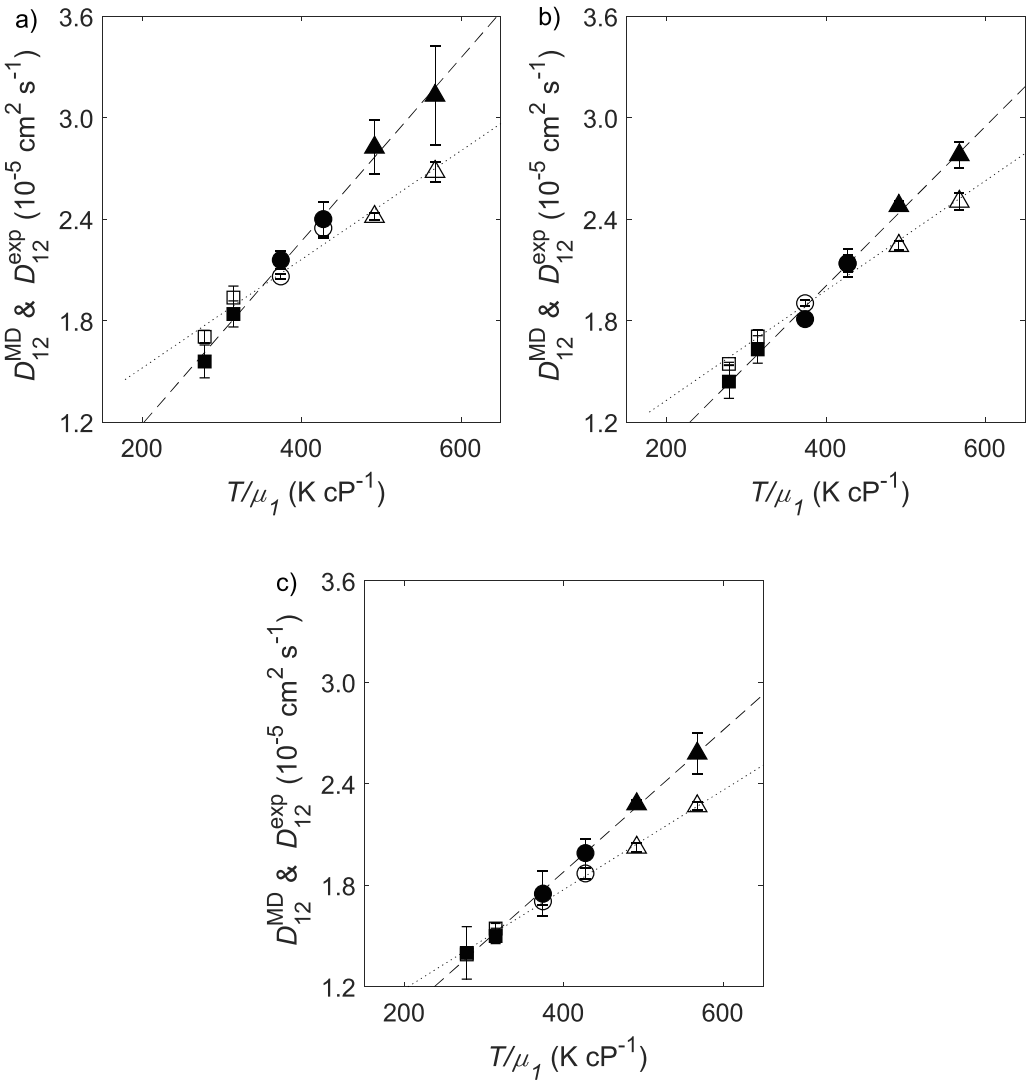

Fig. 3. Diffusion coefficients of aldehydes in liquid ethanol against hydrodynamic coordinates: filled symbols are D_{12}^{MD} values; open symbols are D_{12}^{exp} values from Ref. [52]. Values reported at 303.15 K (■ and □), 318.15 K (○ and ●) and 333.15 K (▲ and △) for (a) butanal, (b) pentanal and (c) hexanal. Viscosity values estimated by Mamedov equation as proposed by Cano-Gómez *et al.* [55].

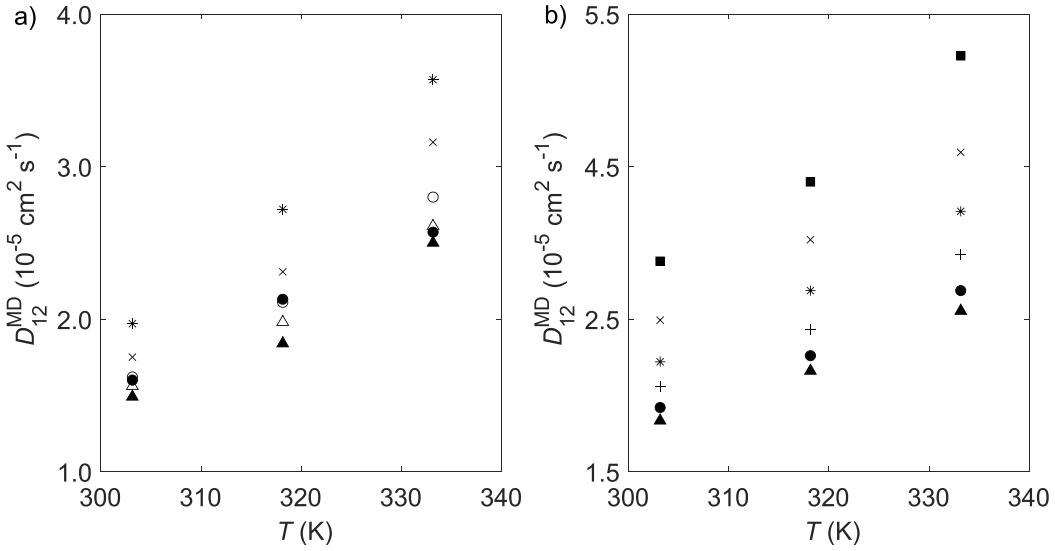

Fig. 4. Computed diffusivities (D_{12}^{MD}) in liquid ethanol against temperature, at 1 bar, for: (a) ketones: acetone (*), butanone (+), pentan-2-one (●), pentan-3-one (○), hexan-2-one (▲), hexan-3-one (△); and (b) aldehydes: methanal (■), ethanal (×). Propanal (*), butanal (+), pentanal (●), hexanal (▲).

from MD and it is not translated in clear trends in all cases, as frequently happens with other properties of liquids estimated by phenomenological models.

Within the same chemical family, the analysis of D_{12}^{MD} variation with solute size (see Fig. 4) evidences that as more carbons the molecule contains the lower is the diffusivity, which can be easily expected from the Stokes-Einstein relationship ($D_{12} \propto 1/r$, being r the radius of the "spherical" solute) [56] or from the free-volume theory (increasing the solute diameter at fixed solvent average free volume decreases D_{12}) [6,57].

As reported by Zêzere *et al.* [52], the experimental diffusivities of ketones and aldehydes isomers are statistically different, while for isomeric ketones the D_{12} values are statistically identical. Nonetheless, in the case of computed MD diffusivities, such similarities/differences are only partially confirmed. In fact, as shown in Fig. 5, the D_{12}^{MD} values of isomeric ketones are the same. However, as for ketones and aldehydes isomers, it is clear the overlapping of D_{12}^{MD} values between isomers, meaning that the interactions between the solvent and the different solutes are similar (see next section) and quantitative differences in the calculated diffusivities are difficult to observe. It is worth noting that the experimental diffusivities of the aldehyde and ketone constitutional isomers are only *ca.* 7 % different [52], which is within the uncertainties associated to the calculated data.

The systematic deviations found in the D_{12}^{MD} values in relation to T, which also translates to T/μ_1, motivated us to introduce separate correction equations for the D_{12}^{MD} values of the ketones and aldehydes, which were derived through the minimization of the differences between the calculated and experimental data for propanone (Eq. (11)) and butanal (Eq. (12)), respectively, and where $D_{12}^{MD\ corr}$ is the corrected D_{12}^{MD} value:

$$D_{12}^{MD\ corr} = D_{12}^{MD}\left(-6.755 \times 10^{-4}\frac{T}{\mu_1} + 1.172\right) \quad (11)$$

$$D_{12}^{MD\ corr} = D_{12}^{MD}\left(-8.548 \times 10^{-4}\frac{T}{\mu_1} + 1.314\right) \quad (12)$$

The detailed tabulated results can be found in the Supplementary Data (Tables SD10 and SD11) while graphical representations of $D_{12}^{MD\ corr}$ and D_{12}^{exp} *versus* T/μ_1 are depicted in Figures SD1 and SD2.

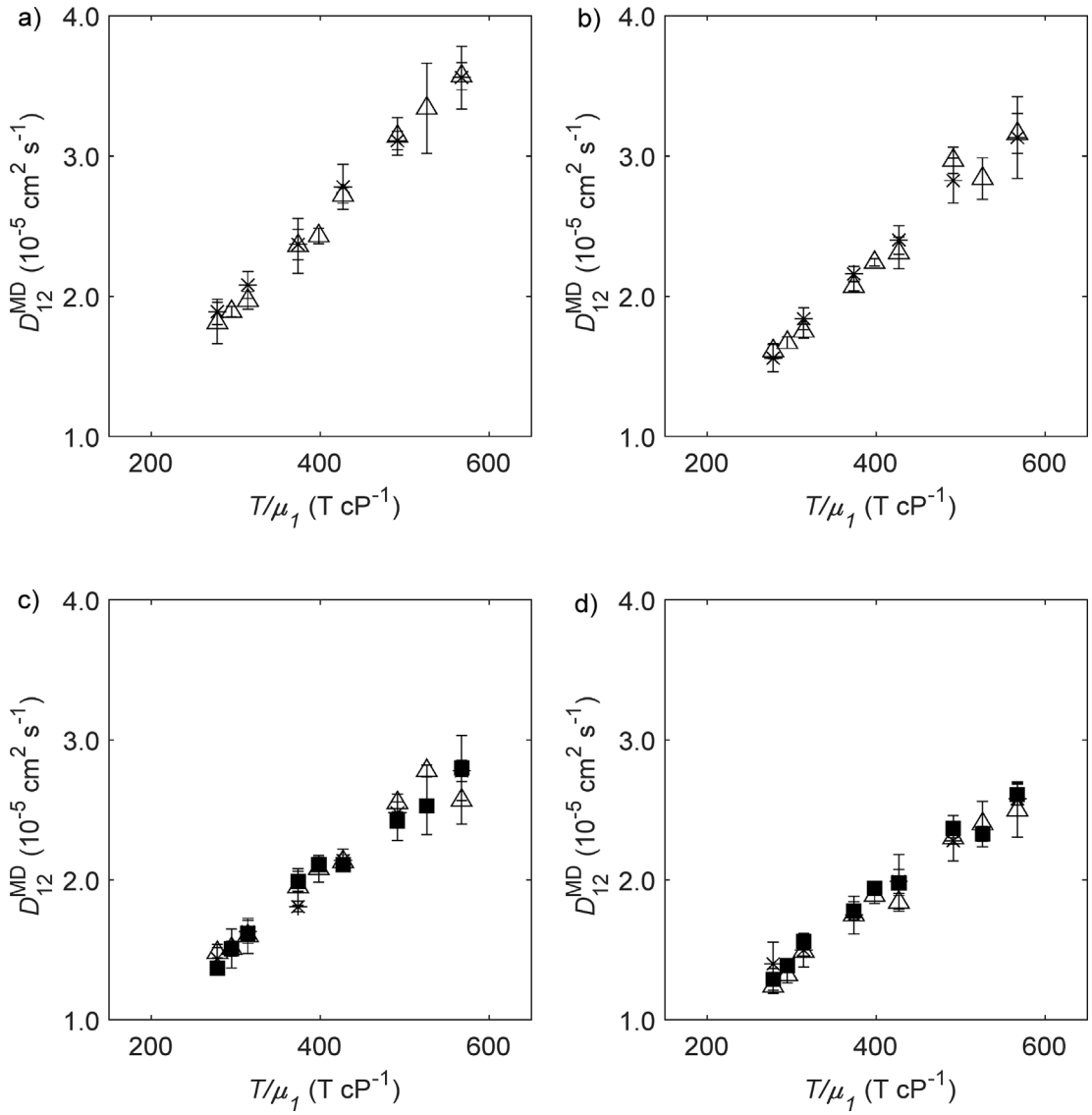

Fig. 5. Computed diffusivities (D_{12}^{MD}) in liquid ethanol against hydrodynamic coordinates for: (a) acetone (×) and propanal (△), (b) butanone (×) and butanal (△), (c) pentan-2-one (×), pentan-3-one (■) and pentanal (△) and (d) hexan-2-one (×), hexan-3-one (■) and hexanal (△).

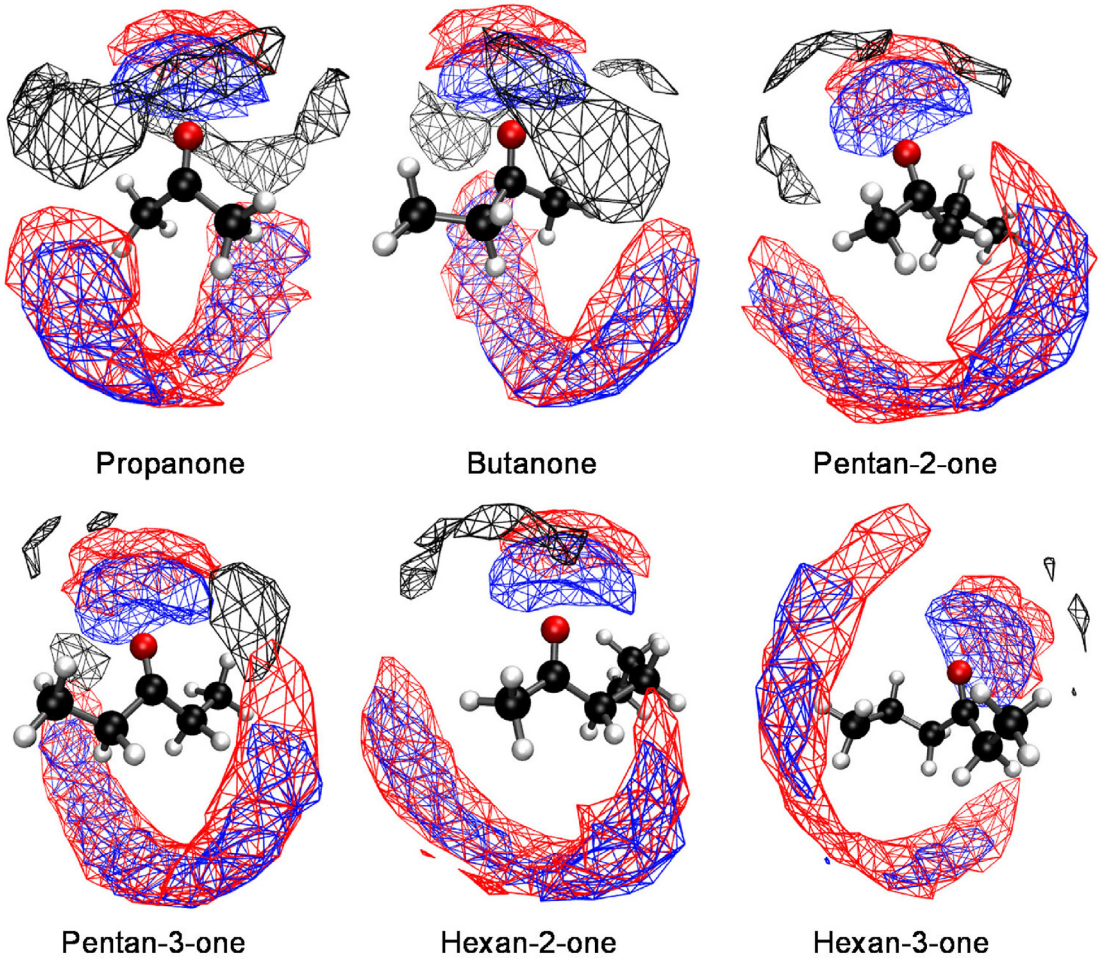

Fig. 6. Spatial distribution functions, at 303.15 K and 1 bar, for the interactions between ketones and atoms of ethanol: ketone···H_{OH} (blue), ketone···O_{OH} (red) and ketone···C_{CH3} (black). Isodensity value of 16 nm^{-3}. (For interpretation of the references to colour in this figure legend, the reader is referred to the web version of this article.)

As it can be seen, the improvements in the calculated diffusivities are clear, with the AARD of the $D_{12}^{MD\ corr}$ values of ketones and aldehydes comprehended in the intervals 1.52 – 5.16 % and 2.94 – 3.45 %, respectively. Notably, the maximum relative deviation values for each family also decreased from 25.32 % to 15.77 % and from 16.94 % to 8.63 %, for ketones and aldehydes, respectively. Alternatively, the relation between RD and T could be addressed by reparameterization of the force field considering the influence of temperature. For example, the temperature-dependence of the density of liquid *n*-dodecane in the study of Klein *et al.* [53] was corrected upon acting on the interaction energy parameter of the L-OPLS-AA force field. However, a similar reparameterization of the force field is beyond the goals of the present study.

3.2. Structural analyses

The dimerization of aldehydes through hydrogen bonding can occur during the simulations and this will impact the calculated diffusivities. The formation of aldehyde dimers was inspected for ethanolic solutions of methanal, butanal and hexanal, at 303.15 K and 1 bar, upon the calculation of minimum distances between the solute molecules, with the corresponding graphical representations for all possible aldehyde-aldehyde pairs being shown in Figure SD3. These three systems were chosen for covering the different alkyl chain sizes in the aldehydes considered. The graphical representations in Figure SD3 clearly show that some solute molecules approach to other solute molecules to distances that are compatible with hydrogen bonding and formation of dimers and that such contacts are not permanent. Moreover, the number of contacts (dimer formation) is non-negligible and increase with the decrease of the alkyl chain size, *i.e.*, contacts are more frequent in the case of methanal (Figure SD3a), and they decrease on going to butanal (Figure SD3b), and, finally, to hexanal (Figure SD3c). However, the visual inspection of Figure SD3 is biased by the different number of solute molecules considered in each case (Table SD5). Therefore, we introduce a new parameter, the so-called dimerization time percentage (DTP), which estimates the fraction of dimer formation along the MD simulation through the following equation:

$$DTP = (TCT/(ST \times NPC)) \times 100 \quad (13)$$

where ST is the simulation time (3 ns, horizontal axis of Figure SD3), NPC is the number of possible contacts (equals to the number of curves in Figure SD3 panels) and TCT stands for the total contact time, which is the sum of the simulation times of the curves in Figure SD3 where two solute molecules are found within a cutoff distance. We considered two values, 0.35 nm, which is the value of the cutoff used for analyzing hydrogen bonds with the *hbond* tool of GROMACS, and 0.5 nm, which is a conservative value for the radius at which the radial distribution functions, RDFs, tend to 1, as can be seen in the analyses below. The calculated DTP values are reported in Table SD12 and, as can be found for the three systems considered, they are <1 %, with either of the cut-off values considered. There-

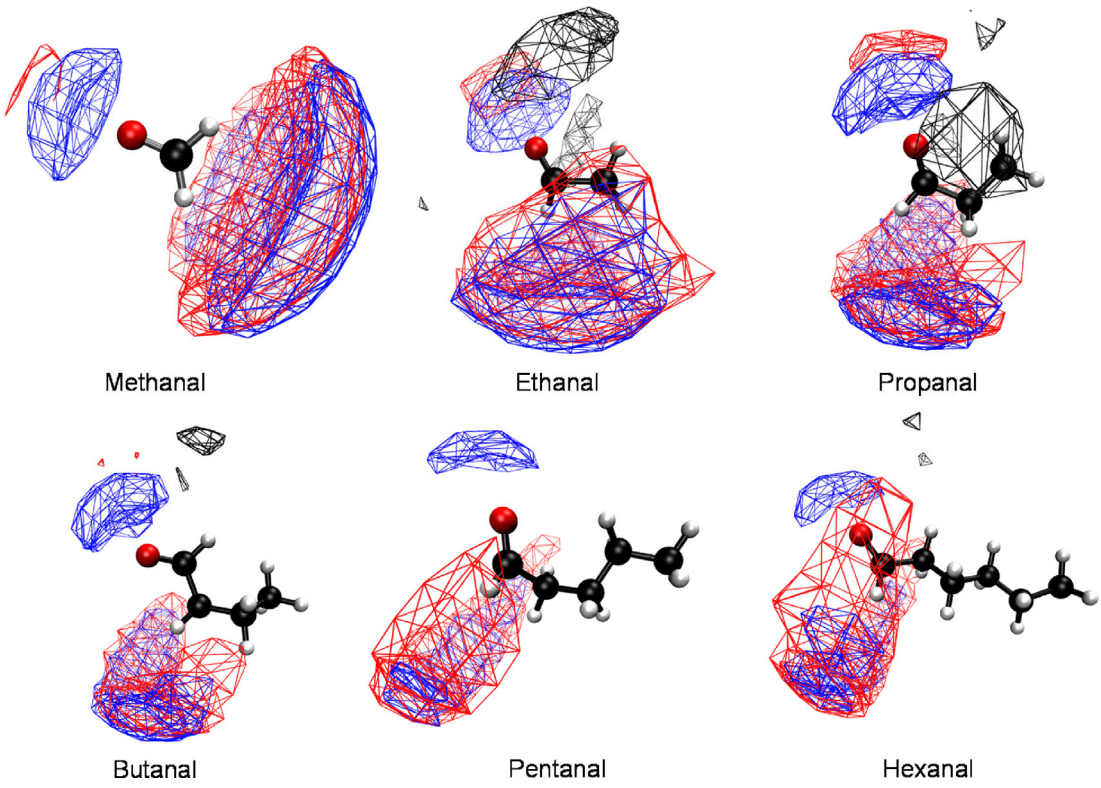

Fig. 7. Spatial distribution functions, at 303.15 K and 1 bar, for the interactions between aldehydes and atoms of ethanol: aldehyde···H_{OH} (blue), aldehyde···O_{OH} (red) and aldehyde···C_{CH3} (black). Isodensity value of 16 nm^{-3}. (For interpretation of the references to colour in this figure legend, the reader is referred to the web version of this article.)

Table 3
Coordination numbers (C_n) of the studied solute-ethanol $O_{\dot{C}=O}H_{OH}$ interaction as function of temperature and pressure. C_n values taken at $r = 0.29$ nm.

Solute	303 K 1 bar	303 K 150 bar	318 K 1 bar	318 K 150 bar	333 K 1 bar	333 K 150 bar
Propanone	0.600	0.597	0.633	0.633	0.642	0.642
Butanone	0.609	0.612	0.631	0.637	0.646	0.646
Pentan-2-one	0.600	0.600	0.615	0.631	0.640	0.629
Pentan-3-one	0.613	0.621	0.629	0.643	0.643	0.638
Hexan-2-one	0.596	0.605	0.627	0.625	0.636	0.629
Hexan-3-one	0.599	0.608	0.608	0.620	0.631	0.636
Methanal	0.449	0.456	0.482	0.479	0.507	0.503
Ethanal	0.491	0.487	0.523	0.523	0.536	0.540
Propanal	0.492	0.499	0.511	0.520	0.534	0.532
Butanal	0.471	0.478	0.503	0.509	0.521	0.532
Pentanal	0.475	0.475	0.494	0.508	0.525	0.523
Hexanal	0.480	0.486	0.510	0.517	0.521	0.531

fore, these results support that most of the time, the solute molecules are surrounded by ethanol molecules and that the effect of dimerization in the calculated results must be small and within the uncertainties associated with the calculations. The excellent agreement between calculated and experimental diffusivities is clearly supportive of this analysis.

The obtained D_{12}^{MD} values will be now analyzed in terms of the structural properties of the systems, namely, the calculated spatial distribution function (SDF) and coordination numbers (C_n) between the solute and the solvent molecules.

Figs. 6 and 7 illustrate the spatial distribution functions corresponding to the interactions of the ketones and aldehydes with the H_{OH}, O_{OH} and C_{CH3} atoms of ethanol in simulations at 303.15 K and 1 bar.

As can be observed, the SDFs reveal clear hydrogen bonding of the type $O_{\dot{C}=O}H_{OH}$, with the ethanol hydrogen atom (blue) closer to the solute C=O than its oxygen atom (red). Interestingly, in the case of the C4 and C6 aldehydes, the red region is not present in the vicinity of the C=O group, which suggests that the hydrogen bond is "less rigid". In all cases, clear red and blue clouds are found in the region opposite to the C=O bond, with the interactions involving the ethanol oxygen atom (red) appearing at shorter distance, indicative of an interaction of the type $[O_{ethanol}]\cdots C{=}O$. The SDFs for the ethanol methyl group support the previous analyses (*cf.* Figures SD4 and SD5).

The coordination numbers (C_n) calculated for the solute-ethanol $O_{\dot{C}=O}H_{OH}$ interaction at $r = 0.29$ nm (average value corresponding to the end of the first peak in the corresponding RDFs) are reported in Table 3 and Fig. 8.

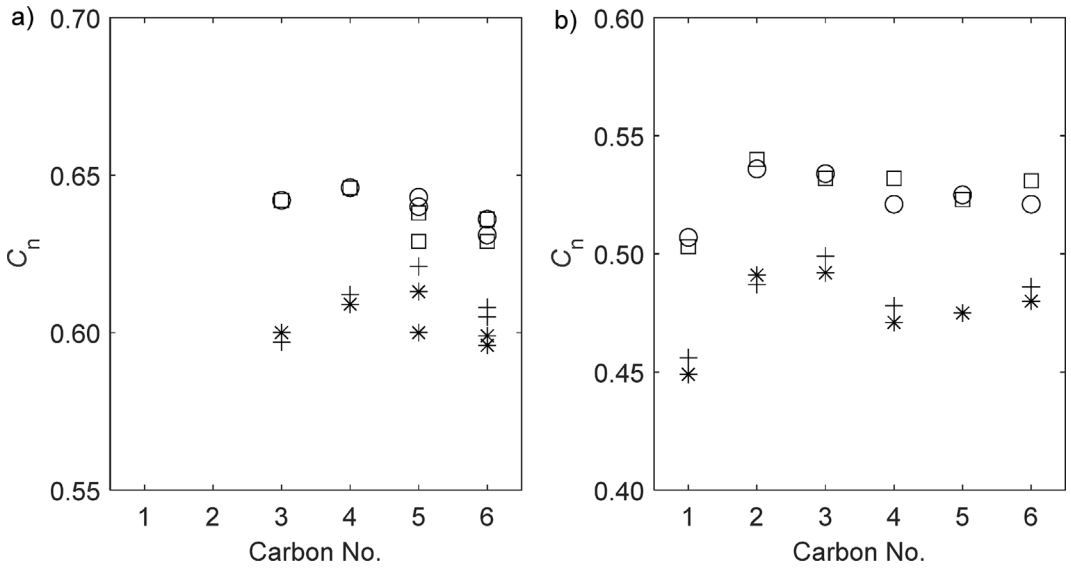

Fig. 8. Coordination numbers (C_n) *versus* number of carbons of the studied (a) ketones and (b) aldehydes at: (*) 303.15 K and 1 bar; (+) 303.15 K and 150 bar; (○) 333.15 K and 1 bar; and (□) 333.15 K and 150 bar. C_n values were calculated from the integration of the radial distribution functions up to $r = 0.29$ nm (average value of the first peak ending).

The influence of temperature, pressure and solute type in the calculated C_n are additionally inspected by performing an analysis of variance (ANOVA; 95 % confidence interval). The results compiled in Table SD13 show that the C_n values vary with T, P and solute type individually, and also with the combined effect of temperature and solute (p-value < 0.05). From Table SD13 and Fig. 8 it is clear that C_n increases with temperature, indicating that more H_{OH} ethanol atoms interact with $O_{C=O}$ atoms from the solute in the first sphere of coordination. As for the effect of pressure on C_n, it is found in most cases that, at constant T, the coordination number slightly increases with P, indicating that the solute–solvent interactions are privileged. Furthermore, such effect seems to be attenuated at higher temperature, since at 333.15 K pressure has almost no influence upon C_n. Regarding the effect of the solute type, ketones exhibit similar C_n values under the same conditions, and an equivalent behavior is found in the case of aldehydes. The exception is methanal that presents lower C_n values in comparison with the remaining aldehydes (see Fig. 8 and Table 3). Comparing aldehydes and ketones, it is always observed that C_n(aldehydes) < C_n(ketones) under equivalent conditions, which indicates that there are more H_{OH} atoms around the $O_{C=O}$ in the first sphere of coordination (*i.e.*, first peak in the RDFs, Figures SD6-SD9) of ketones than of aldehydes. For example, the RDFs of hexanal, hexan-2-one and hexane-3-one plotted in Figure SD9 emphasize this conclusion, because it is clear that the $O_{\dot{C}=O}H_{OH}$ interactions are more relevant in ketones than in aldehydes. When combined with the fact that isomeric aldehydes are smaller than their ketones constitutional isomers, because aldehydes have smaller Lennard-Jones diameter values as discussed in Ref. [52], this observation is coherent with the experimental finding that the diffusivities of aldehydes are higher. If an inferior number of solvent molecules are found in the vicinity of the aldehyde, the latter can more easily move through the solvent than the corresponding ketone. Similar conclusions arise from the RDFs (Figures SD6-SD8) and C_n values (Table 3) calculated for the C3, C4 and C5 solutes.

4. Conclusions

A computational strategy based on molecular dynamics simulations was analyzed in the prediction of tracer diffusion coefficients (D_{12}) of ketones and aldehydes with up to six carbon atoms – propanone, butanone, pentan-2-one, pentan-3-one, hexan-2-one, hexan-3-one, methanal, ethanal, propanal, butanal, pentanal and hexanal – in liquid ethanol at temperatures from 303.15 K to 333.15 K and pressures up to 150 bar.

For ketones, the deviations to experimental data expressed in terms of AARDs lie between 9.48 % and 12.18 %, and for aldehydes between 6.30 % and 9.11 %, which means the MD approach can be successfully applied to estimate diffusion coefficients of such compounds in liquid ethanol.

From the analysis of the dependence of D_{12}^{MD} on temperature, pressure and solute size, the following conclusions can be drawn: (i) While the computed D_{12}^{MD} follows the expected trend with temperature, the relative deviations to the experimental data increase when moving away from 298.15 K; (ii) The computed D_{12}^{MD} values are not always decreasing with pressure as theoretically expected, especially when small increments of pressure are considered, which dues to the weak influence of this operating variable in the case of liquids; (iii) The solute size increment (*i.e.*, the number of carbon atoms in the molecule chain) leads to the decrease of D_{12}^{MD}; (iv) The D_{12}^{MD} of ketones and aldehydes with the same molecular weight are similar at the same conditions. A correction to the computed D_{12}^{MD} was also introduced, which decreased the AARDs of ketones to the range of 1.52 % – 5.16 % and aldehydes to the range of 2.94 % – 3.45 %.

Furthermore, the structural analysis of the simulations evidence that ethanol has more affinity with ketones than aldehydes. Although this is not clearly conveyed to the computed D_{12}^{MD}, it may justify why the experimental diffusivities of ketones are always lower than those of their isomeric aldehydes.

CRediT authorship contribution statement

Bruno Zêzere: Methodology, Investigation, Writing – original draft. **Inês Portugal:** Writing – review & editing, Formal analysis. **Carlos M. Silva:** Supervision, Conceptualization, Resources, Writing – review & editing, Funding acquisition, Formal analysis. **José R.B. Gomes:** Supervision, Resources, Conceptualization, Formal analysis, Writing – review & editing.

Data availability

The raw/processed data required to reproduce the above findings cannot be shared at this time due to technical/time limitations.

Declaration of Competing Interest

The authors declare that they have no known competing financial interests or personal relationships that could have appeared to influence the work reported in this paper.

Acknowledgements

This work was developed within the scope of the project CICECO-Aveiro Institute of Materials, UIDB/50011/2020, UIDP/50011/2020 and LA/P/0006/2020, financed by national funds through the FCT/MEC (PIDDAC). Bruno Zêzere thanks FCT for the PhD grant SFRH/BD/137751/2018.

Appendix A. Supplementary data

Force field parameters (Tables SD1-SD4), number of solute molecules used for each system simulated (Tables SD5), cutoff radius test (Table SD6), density values from MD (Table SD7), MD diffusivities using different fitting regions (Table SD8), simulation length test (Table SD9), corrected MD diffusivities (Tables SD10-SD11), dimerization time percentages (Tables SD12), analysis of variance (Table SD13), Stokes-Einstein representations (Figs. SD1-SD2), minimum distance representations (Fig. SD3) spatial distribution functions (Figs. SD4-SD5) and radial distribution functions (Figs. SD6-SD9). Supplementary data to this article can be found online at https://doi.org/10.1016/j.molliq.2022.121068.

References

[1] R. Taylor, R. Krishna, Multicomponent mass transfer, Wiley Series in Chemical Engineering, John Wiley & Sons Inc, New York, 1993.
[2] E.L.G. Oliveira, A.J.D. Silvestre, C.M. Silva, Review of kinetic models for supercritical fluid extraction, Chem. Eng. Res. Des. 89 (2011) 1104–1117, https://doi.org/10.1016/j.cherd.2010.10.025.
[3] B. Zêzere, I. Portugal, J.R.B. Gomes, C.M. Silva, Revisiting Tracer Liu-Silva-Macedo model for binary diffusion coefficient using the largest database of liquid and supercritical systems, J. Supercrit. Fluids. 168 (2021), https://doi.org/10.1016/j.supflu.2020.105073.
[4] A.L. Magalhães, S.P. Cardoso, B.R. Figueiredo, F.A. Da Silva, C.M. Silva, Revisiting the Liu-Silva-Macedo model for tracer diffusion coefficients of supercritical, liquid, and gaseous systems, Ind. Eng. Chem. Res. 49 (2010) 7697–7700, https://doi.org/10.1021/ie1009475.
[5] H. Liu, C.M. Silva, E.A. Macedo, New equations for tracer diffusion coefficients of solutes in supercritical and liquid solvents based on the Lennard-Jones fluid model, Ind. Eng. Chem. Res. 36 (1997) 246–252, https://doi.org/10.1021/ie9602318.
[6] C.M. Silva, H. Liu, E.A. Macedo, Models for self-diffusion coefficients of dense fluids, including hydrogen-bonding substances, Chem. Eng. Sci. 53 (1998) 2423–2429, https://doi.org/10.1016/S0009-2509(98)00037-2.
[7] J.H. Dymond, Corrected Enskog theory and the transport coefficients of liquids, J. Chem. Phys. 60 (1974) 969–973, https://doi.org/10.1063/1.1681175.
[8] C.M. Silva, H. Liu, Modelling of Transport Properties of Hard Sphere Fluids and Related Systems, and its Applications, in: Á. Mulero (Ed.), Lecture Notes in Physics Theory and Simulation of Hard-Sphere Fluids and Related Systems, Springer Berlin Heidelberg, Berlin, Heidelberg, 2008, pp. 383–492.
[9] C.R. Wilke, P. Chang, Correlation of diffusion coefficients in dilute solutions, AIChE J. 1 (1955) 264–270, https://doi.org/10.1002/aic.690010222.
[10] H. Liu, E. Ruckenstein, Predicting the diffusion coefficients in supercritical fluids, Ind. Eng. Chem. Res. 36 (1997) 888–895, https://doi.org/10.1021/ie9604381.
[11] B. Zêzere, I. Portugal, J.R.B. Gomes, C.M. Silva, Modeling tracer diffusion coefficients of any type of solutes in polar and non-polar dense solvents, Materials. 15 (2022) 6416, https://doi.org/10.3390/ma15186416.
[12] J.P.S. Aniceto, B. Zêzere, C.M. Silva, Machine learning models for the prediction of diffusivities in supercritical CO_2 systems, J. Mol. Liq. (2021), https://doi.org/10.1016/j.molliq.2021.115281.
[13] J.P.S. Aniceto, B. Zêzere, C.M. Silva, Predictive models for the binary diffusion coefficient at Iinfinite dilution in polar and nonpolar fluids, Materials. 14 (2021) 542, https://doi.org/10.3390/ma14030542.
[14] J.P. Allers, J.A. Harvey, F.H. Garzon, T.M. Alam, Machine learning prediction of self-diffusion in Lennard-Jones fluids, J. Chem. Phys. 153 (2020), https://doi.org/10.1063/5.0011512.
[15] R.V. Vaz, A.L. Magalhães, D.L.A. Fernandes, C.M. Silva, Universal correlation of self-diffusion coefficients of model and real fluids based on residual entropy scaling law, Chem. Eng. Sci. 79 (2012) 153–162, https://doi.org/10.1016/j.ces.2012.05.006.
[16] D. Bellaire, O. Großmann, K. Münnemann, H. Hasse, Diffusion coefficients at infinite dilution of carbon dioxide and methane in water, ethanol, cyclohexane, toluene, methanol, and acetone: A PFG-NMR and MD simulation study, J. Chem. Thermodyn. 166 (2022), https://doi.org/10.1016/j.jct.2021.106691.
[17] T. Kulschewski, J. Pleiss, A molecular dynamics study of liquid aliphatic alcohols: simulation of density and self-diffusion coefficient using a modified OPLS force field, Mol. Simul. 39 (2013) 754–767, https://doi.org/10.1080/08927022.2013.769680.
[18] M.C. Barrera, M. Jorge, A polarization-consistent model for alcohols to predict solvation free energies, J. Chem. Inf. Model. 60 (2020) 1352–1367, https://doi.org/10.1021/acs.jcim.9b01005.
[19] R.V. Vaz, J.R.B. Gomes, C.M. Silva, Molecular dynamics simulation of diffusion coefficients and structural properties of ketones in supercritical CO_2 at infinite dilution, J. Supercrit. Fluids. 107 (2016) 630–638, https://doi.org/10.1016/J.SUPFLU.2015.07.025.
[20] X. He, Y. Zhu, A. Epstein, Y. Mo, Statistical variances of diffusional properties from ab initio molecular dynamics simulations, Npj Comput. Mater. 4 (2018) 18, https://doi.org/10.1038/s41524-018-0074-y.
[21] M.P. Allen, D.J. Tildesley, Computer Simulation of Liquids, Oxford University Press (2017), https://doi.org/10.1093/oso/9780198803195.001.0001.
[22] W.L. Jorgensen, D.S. Maxwell, J. Tirado-Rives, Development and testing of the OPLS all-atom force field on conformational energetics and properties of organic liquids, J. Am. Chem. Soc. 118 (1996) 11225–11236, https://doi.org/10.1021/ja9621760.
[23] M.M. Reif, P.H. Hünenberger, C. Oostenbrink, New interaction parameters for charged amino acid side chains in the GROMOS force field, J. Chem. Theory Comput. 8 (2012) 3705–3723, https://doi.org/10.1021/ct300156h.
[24] J. Wang, W. Wang, P.A. Kollman, D.A. Case, Automatic atom type and bond type perception in molecular mechanical calculations, J. Mol. Graph. Model. 25 (2006) 247–260, https://doi.org/10.1016/j.jmgm.2005.12.005.
[25] I. Skarmoutsos, I.D. Petsalakis, J. Samios, The polar cosolvent effect on caffeine solvation in supercritical CO_2–ethanol mixtures: A molecular modeling approach, Ind. Eng. Chem. Res. 60 (2021) 11834–11847, https://doi.org/10.1021/acs.iecr.1c00956.
[26] H. Lee, M. Ostadhassan, Z. Sun, H. Pu, B. Liu, R.S. Varma, H.W. Jang, M. Shokouhimher, Diffusivity and hydrophobic hydration of hydrocarbons in supercritical CO_2 and aqueous brine, RSC Adv. 10 (2020) 37938–37946, https://doi.org/10.1039/D0RA06499H.
[27] S.P. Khanal, N.P. Adhikari, Thermodynamic and transport properties of amoxicillin, J. Mol. Liq. 354 (2022), https://doi.org/10.1016/j.molliq.2022.118865.
[28] G. Guevara-Carrion, R. Fingerhut, J. Vrabec, Diffusion in multicomponent aqueous alcoholic mixtures, Sci. Rep. 11 (2021) 12319, https://doi.org/10.1038/s41598-021-91727-w.
[29] K.K. Liong, P.A. Wells, N.R. Foster, Diffusion in supercritical fluids, J. Supercrit. Fluids. 4 (1991) 91–108, https://doi.org/10.1016/0896-8446(91)90037-7.
[30] D. Bellaire, K. Münnemann, H. Hasse, Mutual diffusion coefficients from NMR imaging, Chem. Eng. Sci. 255 (2022), https://doi.org/10.1016/j.ces.2022.117655.
[31] G. Taylor, Dispersion of soluble matter in solvent flowing slowly through a tube, Proc. R. Soc. A Math. Phys, Eng. Sci. 219 (1953) 186–203, https://doi.org/10.1098/rspa.1953.0139.
[32] G. Taylor, Diffusion and mass transport in tubes, Proc. Phys. Soc. Sect. B. 67 (1954) 857–869, https://doi.org/10.1088/0370-1301/67/12/301.
[33] G. Taylor, The dispersion of matter in turbulent flow through a pipe, Proc. R. Soc. A Math. Phys, Eng. Sci. 223 (1954) 446–468, https://doi.org/10.1098/rspa.1954.0130.
[34] R. Aris, On the dispersion of a solute by diffusion, convection and exchange between phases, Proc. R. Soc. A Math. Phys. Eng. Sci. 252 (1959) 538–550, https://doi.org/10.1098/rspa.1959.0171.
[35] B. Zêzere, J. Iglésias, I. Portugal, J.R.B. Gomes, C.M. Silva, Diffusion of quercetin in compressed liquid ethyl acetate and ethanol, J. Mol. Liq. (2020), https://doi.org/10.1016/j.molliq.2020.114714.
[36] G. Cai, W. Katsumata, I. Okajima, T. Sako, T. Funazukuri, C.Y. Kong, Determination of diffusivities of triolein in pressurized liquids and in supercritical CO_2, J. Mol. Liq. 354 (2022), https://doi.org/10.1016/j.molliq.2022.118860.
[37] T. Funazukuri, C.Y. Kong, S. Kagei, Impulse response techniques to measure binary diffusion coefficients under supercritical conditions, J. Chromatogr. A. 1037 (2004) 411–429, https://doi.org/10.1016/j.chroma.2004.03.043.
[38] T. Funazukuri, C.Y. Kong, S. Kagei, Measurements of binary diffusion coefficients for some low volatile compounds in supercritical carbon dioxide by input–output response technique with two diffusion columns connected in

series, Fluid Phase Equilib. 194 (2002) 1169–1178, https://doi.org/10.1016/S0378-3812(01)00717-8.
[39] E. Lindahl, M.J. Abraham, B. Hess, D. van der Spoel, GROMACS 2019.3 Manual, 2019. Doi: 10.5281/zenodo.3243834.
[40] E. Lindahl, M.J. Abraham, B. Hess, D. Van Der Spoel, GROMACS 2019.3 Source code, (2019). Doi: 10.5281/zenodo.3243833.
[41] M.J. Abraham, T. Murtola, R. Schulz, S. Páll, J.C. Smith, B. Hess, E. Lindahl, GROMACS: High performance molecular simulations through multi-level parallelism from laptops to supercomputers, SoftwareX. 1–2 (2015) 19–25, https://doi.org/10.1016/j.softx.2015.06.001.
[42] F.D. Lenahan, M. Piszko, T. Klein, A.P. Fröba, Diffusivities in binary mixtures of *n*-decane, *n*-hexadecane, *n*-octacosane, 2-methylpentane, 2,2-dimethylbutane, cyclohexane, benzene, ethanol, 1-decanol, ethyl butanoate, or *n*-hexanoic acid with dissolved He or Kr close to infinite dilution, J. Chem. Eng. Data. 67 (2022) 622–635, https://doi.org/10.1021/acs.jced.1c00922.
[43] H.J.C. Berendsen, J.P.M. Postma, W.F. van Gunsteren, A. DiNola, J.R. Haak, Molecular dynamics with coupling to an external bath, J. Chem. Phys. 81 (1984) 3684–3690, https://doi.org/10.1063/1.448118.
[44] R. Hockney, S. Goel, J. Eastwood, Quiet high-resolution computer models of a plasma, J. Comput. Phys. 14 (1974) 148–158, https://doi.org/10.1016/0021-9991(74)90010-2.
[45] G. Bussi, D. Donadio, M. Parrinello, Canonical sampling through velocity rescaling, J. Chem. Phys. 126 (2007), https://doi.org/10.1063/1.2408420.
[46] M. Parrinello, A. Rahman, Polymorphic transitions in single crystals: A new molecular dynamics method, J. Appl. Phys. 52 (1981) 7182–7190, https://doi.org/10.1063/1.328693.
[47] U. Essmann, L. Perera, M.L. Berkowitz, T. Darden, H. Lee, L.G. Pedersen, A smooth particle mesh Ewald method, J. Chem. Phys. 103 (1995) 8577–8593, https://doi.org/10.1063/1.470117.
[48] DDBST GmbH, Compressibility (isothermal) of Ethanol. http://www.ddbst.com/en/EED/PCP/CMPT_C11.php (accessed March 18, 2022).
[49] C.K. Zéberg-Mikkelsen, L. Lugo, J. Fernández, Density measurements under pressure for the binary system (ethanol+methylcyclohexane), J. Chem. Thermodyn. 37 (2005) 1294–1304, https://doi.org/10.1016/j.jct.2005.03.016.
[50] V.I. Deshchenya, N.D. Kondratyuk, A.V. Lankin, G.E. Norman, Molecular dynamics study of sucrose aqueous solutions: From solution structure to transport coefficients, J. Mol. Liq. 367 (2022), https://doi.org/10.1016/j.molliq.2022.120456.
[51] S.H. Jamali, Transport Properties of Fluids: Methodology and Force Field Improvement using Molecular Dynamics Simulations, Delft University of Technology (2020), https://doi.org/10.4233/uuid:c32e495d-5dd9-42f8-9203-b540e1f9f175.
[52] B. Zêzere, S. Buchgeister, S. Faria, I. Portugal, J.R.B. Gomes, C.M. Silva, Diffusivities of linear unsaturated ketones and aldehydes in compressed liquid ethanol, J. Mol. Liq. 367 (2022), https://doi.org/10.1016/j.molliq.2022.120480.
[53] T. Klein, F.D. Lenahan, M. Kerscher, M.H. Rausch, I.G. Economou, T.M. Koller, A. P. Fröba, Characterization of long linear and branched alkanes and alcohols for temperatures up to 573.15 K by surface light scattering and molecular dynamics simulations, J. Phys. Chem. B. 124 (2020) 4146–4163, https://doi.org/10.1021/acs.jpcb.0c01740.
[54] H. Baba, R. Urano, T. Nagai, S. Okazaki, Prediction of self-diffusion coefficients of chemically diverse pure liquids by all-atom molecular dynamics simulations, J. Comput. Chem. 43 (2022) 1892–1900, https://doi.org/10.1002/jcc.26975.
[55] J.J. Cano-Gómez, G.A. Iglesias-Silva, M. Ramos-Estrada, Correlations for the prediction of the density and viscosity of 1-alcohols at high pressures, Fluid Phase Equilib. 404 (2015) 109–117, https://doi.org/10.1016/j.fluid.2015.06.042.
[56] R.C. Reid, J.M. Prausnitz, B.E. Poling, The Properties of Gases and Liquids, Fourth ed., McGraw-Hill International Editions, New York, 1987.
[57] H. Liu, C.M. Silva, E.A. Macedo, Generalised free-volume theory for transport properties and new trends about the relationship between free volume and equations of state, Fluid Phase Equilib. 202 (2002) 89–107, https://doi.org/10.1016/S0378-3812(02)00083-3.